Improving the level of seismic hazard parameters in Saudi Arabia using earthquake location

**Abdullah M. Al-Amri · Arthur J. Rodgers ·
Tariq A. Al-Khalifah**

Abstract Saudi Arabia is characterized as largely aseismic; however, the tectonic plate boundaries that surround it are very active. To improve characterization of seismicity and ground motion hazard, the Saudi Arabian Digital Seismic Network (SANDSN) was installed in 1998 and continues to be operated by the Saudi Geological Survey (SGS) and King Abdulaziz City for Science and Technology (KACST). This article describes research performed to improve seismic hazard parameters using earthquake location and magnitude calibration of the high-quality SANDSN data. The SANDSN consists of 38 seismic stations, 27 broadband, and 11 short period. All data are telemetered in real time to a central facility at KACST in Riyadh. The SANDSN stations show low background noise levels and have good signal detection capabilities; however, some stations show cultural noise at frequencies above 1.0 Hz. We assessed the SANDSN event location capabilities by comparing KACST locations with well-determined locations derived from ground truth or global observations. While a clear location bias exists when using the global average *iasp91* earth model, the locations can be improved by using regional models optimized for different tectonic source regions. The article presents detailed analysis of some events and Dead Sea explosions where we found gross errors in estimated locations. New velocity models we calculated that should improve estimated locations of regional events in three specific regions include (1) Gulf of Aqabah—Dead Sea region, (2) Arabian Shield, and (3) Arabian Platform. Recently, these models were applied to the SANDSN to improve local and teleseismic event locations and to develop an accurate magnitude scale for Saudi Arabia. The Zagros Thrust presents the most seismic hazard to eastern Saudi Arabia because of the frequent occurrence of earthquakes. Although these events are 200 km or further from the Arabian coast, wave propagation through sedimentary structure of the Gulf causes long-duration ground motions for periods between 3 and 10 s. Such ground motions could excite response in large engineered structures (e.g., tall buildings and long bridges) such as was experienced after the November 22, 2005 Qeshm Island earthquake off the southern coast of Iran.

A. M. Al-Amri (✉)
Department of Geology, King Saud University,
Riyadh, Saudi Arabia
e-mail: amri444@yahoo.com

A. J. Rodgers
Atmospheric, Earth and Energy Department,
Lawrence Livermore National Laboratory,
Livermore, CA 94551, USA
e-mail: rodgers7@llnl.gov

T. A. Al-Khalifah
Research Institute of Astronomy and Geophysics,
King Abdulaziz City for Science and Technology,
Riyadh, Saudi Arabia

Introduction

There has been only a modest body of research on earthquake seismology of Arabian Peninsula compared to the vast body of work on petroleum geology and geophysics of the Arabian Platform. This is due to the relative absence of recording stations and earthquakes within the Arabian interior. Seismic networks have operated within or adjacent to the Arabian Peninsula, but these networks have lacked spatial coverage and/or three-

component digital instrumentation to characterize wave propagation, attenuation, and seismicity. Furthermore, most networks have lacked broadband stations, which can be used for source and earth structure investigations.

Consequently, the main objective of this study was to evaluate SANDSN noise levels and location biases, and obtain new constraints on crustal and upper mantle structure for improving seismic hazard assessment in Saudi Arabia using data obtained by the SANDSN. These data demonstrate the value broadband recording and data analysis.

The article attempts to improve estimates of earthquake locations by using broadband waveform data from the SANDSN. In the following, we present a brief summary of investigations of seismotectonics and structure of the Arabian Peninsula and a description of the SANDSN system. Then, we present the result of new investigations to improve event location. This is followed by ground motion observations and new reports of long-period ground motion hazards in the Arabian Gulf. We conclude with summary remarks and recommendations for future investigations.

Seismotectonics and structure of the Arabian Plate

The Arabian Peninsula forms a single tectonic plate, the Arabian Plate. It is surrounded on all sides by active plate boundaries as evidenced by earthquake locations (Adams and Barazangi 1984). Figure 1 shows a map of the Arabian Peninsula along with major tectonic features and earthquake locations. Earthquake locations, taken from the United States Geologic Survey Preliminary Determination of Epicenters for the period 1990–1999, show that active tectonics of the region is dominated by the collision of the Arabian Plate with the Eurasian Plate along the Zagros and Bitlis Thrust systems, rifting and seafloor spreading in the Red Sea and Gulf of Aden. Strike–slip faulting occurs along the Gulf of Aqabah and Dead Sea Transform fault systems.

The eastern and northern boundaries of the Arabian Plate are characterized by active continental collision of Arabian and Eurasian Plates along the Zagros and Bitlis Thrust systems (Stocklin 1968). Earthquake activity is intense in the Zagros Mountains, a zone of approximately 200 km width including the Zagros Fold Belt and Zagros Thrust Zone (Nowroozi 1972; Berberian 1976; Jackson and McKenzie 1984).
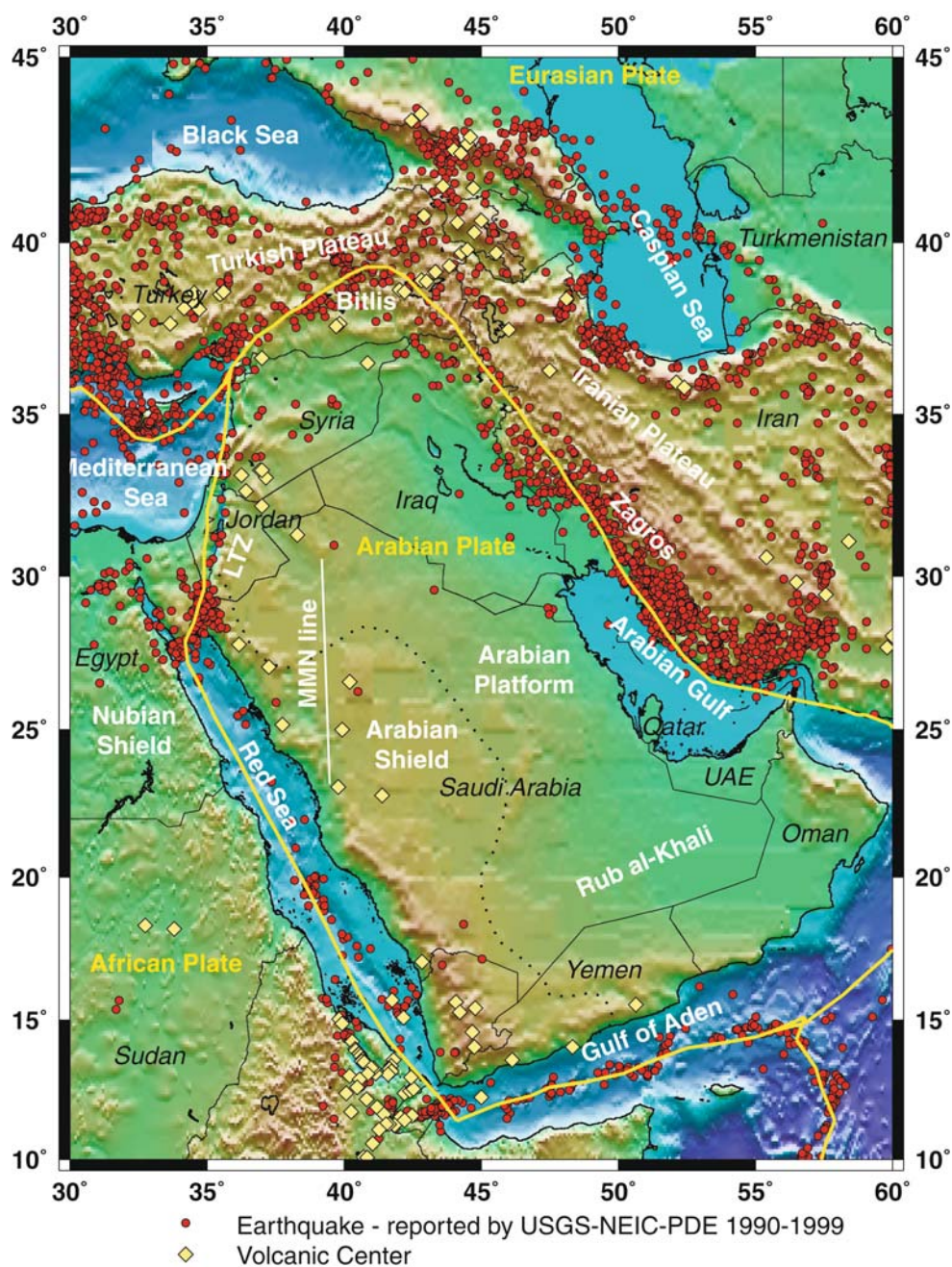
In general, seismicity in the Zagros Mountains is shallow with focal depths ranging not more than 20 km (e.g., Jackson and Fitch 1981; Maggi et al. 2000; Engdahl et al. 2006). The Zagros Thrust system is a prominent source of large earthquakes (Ambraseys and Melville 1982). Large earthquakes in the Zagros Mountains of southern Iran lead to long-period ground motion along the eastern shore of the Arabian Gulf (discussed in a later section).

The plate boundary changes from convergent in the Bitlis Thrust in Turkey to left-lateral strike–slip along the Dead Sea Fault System. This is a major continental strike–slip fault capable of large earthquakes, given the observed offset of ~100 km (Garfunkel 1981; Girdler 1990). The Dead Sea Fault System continues into the Gulf of Aqabah. The intense seismicity in and around the Gulf of Aqabah poses a significant seismic hazard to Saudi Arabia, including large earthquakes and swarm activity in 1983, 1990, 1993, and 1995 (e.g., Ambraseys et al. 1994; Al-Amri 1995; Klinger et al. 1999). The Arabian Plate boundary in the Red Sea is divergent, where continental lithosphere has been ruptured to form new oceanic crust (e.g., Stoeser and Camp 1985). The morphology of the rifted lithosphere has been imaged recently by Hansen et al. (2007) using data from the SANDSN. Deep structure of the Red Sea and Arabian Shield is characterized by low seismic velocities likely associated with upwelling of hot mantle material (Rodgers et al. 1999; Debayle et al. 2001; Benoit et al. 2003; Park et al. 2007). Seafloor spreading is also occurring along the Gulf of Aden (Cochran 1981) with crustal structure typical of passive margins (Tiberi et al. 2007).

The Arabian interior is characterized into two geologic provinces associated with the presence or absence of sedimentary cover. The Arabian Platform (eastern Arabia) is covered by sediments that thicken toward the Arabian Gulf. The Arabian Shield has no appreciable sedimentary cover with many outcrops. Figure 1 shows the approximate boundary between these provinces. A detailed model of sediment thickness, estimated from compiled drill hole, gravity, and seismic reflection data was published by Seber et al. (1997). Volcanic activity (the Harrats) is observed on the Arabian Shield, particularly along the Mecca–Medina–Nafud line (Fig. 1). This is likely to be related to the opening of the Red Sea and mantle asthenospheric upwelling beneath western Arabia (e.g., Camp and Roobol 1992). Estimates of lithospheric structure have come from active source (Mooney et al. 1985; Gettings et al. 1986) and passive (Al-Amri 1998, 1999; Sandvol et al. 1998a, b; Benoit et al. 2003; Al-Damegh et al. 2005; Mohsen et al. 2006; Tkalčič et al. 2006; Hansen et al. 2007; Park et al. 2007) seismological investigations.

Seismic surface waves recorded at the long-period analog stations RYD (Riyadh, Saudi Arabia), SHI (Shiraz, Iran), TAB (Tabriz, Iran), HLW (Helwan, Egypt), AAE (Addis-Ababa, Ethiopia), and JER (Jerusalem) were used to estimate crustal and upper mantle structure (Knopoff and Fouda 1975; Seber and Mitchell 1992). These studies reported fast crustal velocities in the Arabian Shield and slower ones in the Arabian Platform. Stoeser and Camp (1985) and Mooney et al. (1985) suggested that the geological evolution and seismic velocity structure of the

Fig. 1 Map of the Arabian
Peninsula and surrounding
regions. Major geographic and
tectonic/geologic features are
indicated. Approximate plate
boundaries are indicated by
yellow lines. Earthquakes and
volcanic centers are shown as
red circles and *yellow diamond*,
respectively. The approximate
boundary between the Arabian
Shield and Arabian Platform is
indicated by the *dotted line*

Arabian Shield could be modeled in terms of Proterozoic
suturing of island arcs and microcontinents. They inter-
preted the boundary between the eastern Arabian Shield
and Platform as a suture zone that separates crustal blocks
of differing composition, with lower velocities in the
crystalline crust of the Arabian Platform and higher
velocities in the Arabian Shield.

The Saudi Arabian Broadband Deployment (Vernon and
Berger 1998; Al-Amri et al. 1999) provided the first
broadband recordings for the Arabian Shield and Platform.
This deployment consisted of nine broadband, three-

component seismic stations along a similar transect to a
seismic refraction study (Mooney et al. 1985; Gettings et al.
1986; Badri 1991). Data from this deployment resulted in
several reports of crustal and upper mantle structure
(Sandvol et al. 1998a; Mellors and Vernon 1999; Rodgers
et al. 1999; Benoit et al. 2003; Mokhtar et al. 1997). The
crustal model of the western Arabian Platform shows a
slightly higher P-velocity for the upper crust in the Arabian
Shield than in the Platform. Also, the crust of the Platform
appears to be 3–5 km thicker than in the Shield. The Moho
Discontinuity beneath the western Arabian Platform occurs

at a depth of 40–45 km, and the velocity of the upper mantle is about 8.2 km/s (Al-Amri 1998, 1999; Rodgers et al. 1999; Tkalčič et al. 2006).

Generally, the crustal thickness in the Arabian Shield varies from about 15 km in the Red Sea, to 20 km along the Red Sea coast to about 35–40 km in the in central Arabian Shield (Sandvol et al. 1998a; Al-Damegh et al. 2005; Tkalčič et al. 2006). Reports of large-scale seismic tomography (e.g., Debayle et al. 2001) suggest that a low-velocity anomaly in the upper mantle extends laterally beneath the Arabian Shield from the Red Sea in the west to the Shield–Platform boundary in the east. Additionally, Debayle et al. (2001) observed a narrow region of low-velocity beneath the Red Sea and the western edge of the Arabian Shield, extending to 650 km depth. Recent tomographic imaging by Park et al. (2007) using SANDSN data found low velocities extending to 400 km in the upper mantle beneath the southern Red Sea and Arabian Shield, but more normal velocities beneath the northern Red Sea, suggesting different geodynamic connections between rifting of the Red Sea and mantle upwelling in the southern and northern Red Sea.

High-frequency regional S-wave phases are quite different for paths sampling the Arabian Shield than those sampling the Arabian Platform (Mellors and Vernon 1999; Al-Damegh et al. 2004). In particular, the mantle Sn phase is nearly absent for paths crossing parts of the Arabian Shield, while the crustal Lg phase has abnormally large amplitude. This may result from an elastic propagation effect or extremely high mantle attenuation and low crustal attenuation occurring simultaneously or a combination of both. High-frequency Lg does not propagate as efficiently across the Arabian Platform compared to the Shield but Sn does propagate efficiently. This suggests that crustal attenuation is low in the higher velocity crust of the Arabian Shield or sedimentary structure in the Arabian Platform attenuates and disrupts the crustal waveguide for Lg. These observations imply that high-frequency ground motions will propagate with lower attenuation in the Arabian Shield compared to the Arabian Platform.

Results and data analysis

SANDSN location performance

In May 1998, King Abdulaziz City for Science and Technology (KACST) began operating the SANDSN (Al-Amri and Al-Amri 1999). It consists of 38 stations mostly distributed across the Arabian Shield (Fig. 2). The instrumentation features 27 broadband and 11 short-period instruments. The station information is compiled in Table 1. All stations record three-component ground motions at a
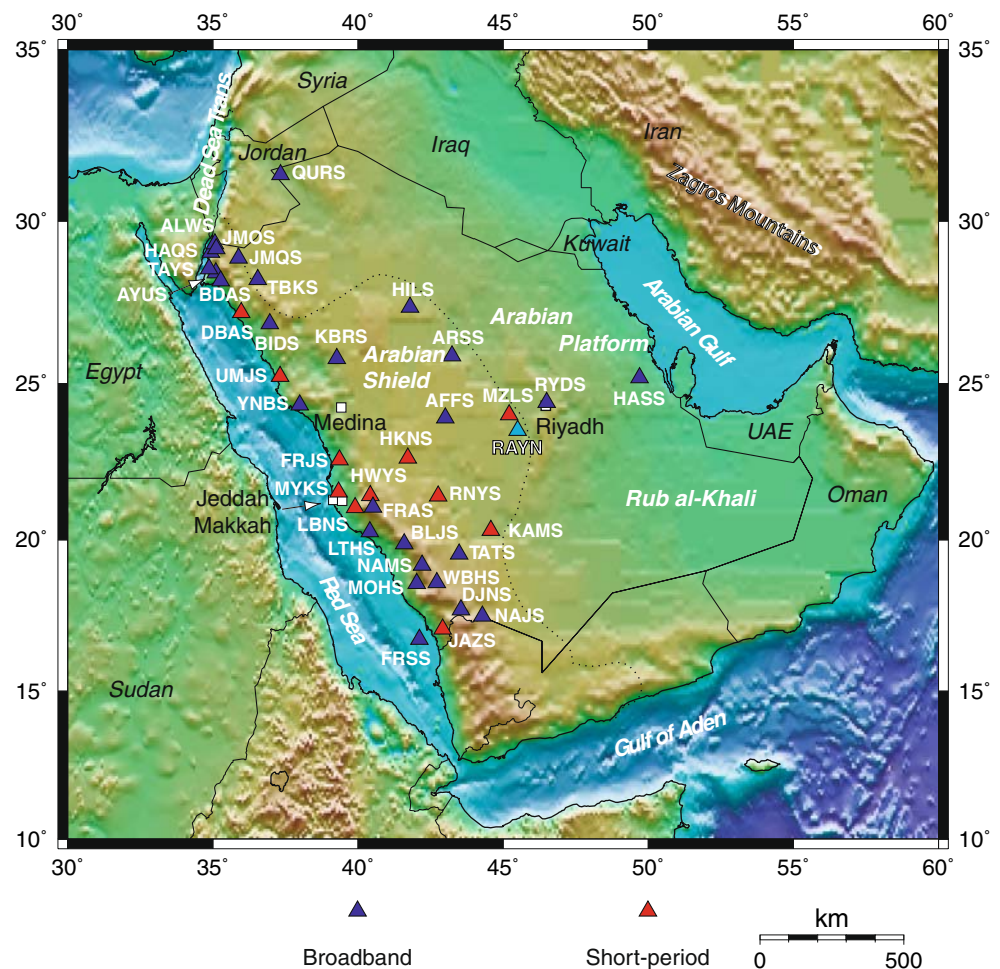
sample rate of 100 samples/second using Quanterra Q730 24-bit data loggers. Broadband and short-period stations operate with Strekeisen STS-2 120-s and Kinemetrics SS-1 Ranger 1-s sensors, respectively. The stations operate continuously and transmit data in real time to the KACST Headquarters in Riyadh. The KACST Data Center receives the raw waveform data and runs the Boulder Real Time Technologies (BRTT) Antelope System. This is a software package for managing real-time seismic network data and performing the basic network operations of detection, association, and location of events as well as data archival. A short-term average-to-long-term average (STA/LTA) energy detector runs continuously and detects phase arrivals. The system attempts to locate the event when a number of arrivals are detected by the network within a specified time window. The system locates events relative to a single global velocity model (iasp91, Kennett and Engdahl 1991). This is a global continental average velocity model derived from worldwide observations of seismic travel times. While this model is appropriate for locating distant (teleseismic) events, it is not necessarily a good model for locating events in and around the Arabian Peninsula. Figure 3 shows the iasp91 model along with lithospheric velocity models from our earlier work (Rodgers et al. 1999; Rodgers et al. 2001). As one can see, iasp91 has no sediment layer, and the crustal thickness (35 km) is thin compared to the Arabian Platform model. There are also differences between the mantle velocities. We will return to these issues later in this study.

The locations of the events outside the network were improved by calibrating the travel time or velocity structure between the event regions and recording stations. The arrival times of moderate-sized events ($m_b \geq 4.5$) can be accurately measured to uncertainties of 1 s or less if noise levels allow for good signal-to-noise levels. The calibration task is made difficult by the fact that one often does not accurately know the location and origin times of events. Earthquakes excite more seismic energy and can be observed at larger distances; however, their locations are more poorly constrained. In some cases where an earthquake is recorded at local distances (<100 km) with good azimuthal coverage, the locations can be accurate to less than 10–20 km (Sweeney 1996). This translates to 1–2 s of travel time at regional distances.

Seismic noise measurements

Background seismic noise is an unavoidable problem in earthquake monitoring. The amplitudes of seismic arrivals decreased with distance and seismic magnitude. Path propagation effects, such as attenuation and elastic structure lead to variability in seismic amplitudes. Noise inhibits the detection of weak seismic arrivals (phases) from distant

Fig. 2 Map of the Saudi Arabian National Digital Seismic Network (SANDSN) seismic station locations. Broadband and short-period stations are indicated by the *blue* and *red triangles*, respectively

and/or small events. Seismic noise is generated from a variety of sources. These include both man-made (e.g., roads and machinery) and natural sources (e.g., wind, ocean waves, and temperature effects). Noise properties can vary between daytime and night hours, and between seasons (e.g., summer and winter). Also, the geologic character of the seismometer placement has a great effect on the noise: Hard-rock sites typically have lower noise levels than those on weathered or sedimentary rock or unconsolidated material. Because of the variety of noise sources, the variability of noise types, site characteristics (e.g., propagation), noise will vary between sites and frequency dependence.

A basic characteristic of seismic network operations is the background noise observed at stations. High background noise inhibits observation of weak signals from small and/or distant events. Broadband stations are particularly sensitive to background noise because they record motions across a broad spectrum, typically 0.01–25 Hz, capturing different noise sources including the microseismic peak at about 0.17 Hz and higher frequency man-made noise. To assess background noise, we measured noise spectra at stations of the SANDSN network. Waveforms were instrument corrected to absolute ground motion using the LLNL developed Seismic Analysis Code (SAC, Goldstein et al. 2003). Noise segments were taken as the available waveform before the P-wave arrival. For noise spectral measurements, we accepted only segments 30 s or longer. This limited the low frequency resolution of our noise estimates. Power spectral densities were computed for noise windows by fast Fourier transform (FFT) and normalized by the window length. Noise spectra are presented in acceleration in decibels relative to 1 $(m/s^2)^2/Hz^2$.

Results for noise at SANDSN stations AFFS and HASS are presented in Figs. 4 and 5, respectively. Shown in each plot are the vertical, north and east component noise acceleration power spectra (in decibels relative to 1 m^2/s^4). Also shown are the average low- and high-noise spectra of Peterson (1993). Results show that station AFFS has the very low noise levels, consistent with the Peterson (1993) low-noise average (Fig. 4). Station HASS have the highest noise levels of the broadband stations (Fig. 5). We found that stations HILS and TATS have very low noise levels, and stations RYDS and QURS have high noise levels.

Table 1 Stations of the Saudi Arabian National Digital Seismic Network (SANDSN)

Station code	Station location	Latitude	Longitude	Elevation (meters)	Sensor type
AFFS	Afif	23.9267	43.0005	109	BB
ALWS	As Safayhah	29.3103	35.0650	0	SP
ARSS	Ar Rass	25.8810	43.2365	72	BB
AYUS	Aynunah	28.1889	35.2689	0	SP
BDAS	Al Bada	28.4317	35.1014	36	BB
BIDS	Al Bida	26.8670	36.9595	0	BB
BLJS	Baljurashi	19.8812	41.5992	206	BB
DBAS	Duba	27.2114	35.9773	18	SP
DJNS	Dahran-Al-Janub	17.7073	43.5434	220	BB
FRAS	Faraa	21.0622	40.5200	0	BB
FRJS	J.-Farasan	22.5905	39.3638	0	SP
FRSS	Farasan Island	16.7392	42.1143	0	BB
HAQS	Haql	29.0548	34.9297	42	BB
HASS	Al Hasa	25.1899	49.6944	20	BB
HILS	Al Hail	27.3835	41.7917	108	BB
HKNS	J.-Hakran	22.6420	41.7158	0	SP
HWYS	Hawiyah	21.4349	40.4177	0	SP
JAZS	Jizan	17.0678	42.9177	0	SP
JMOS	J. Al-Moallq	29.1686	35.1094	0	BB
JMQS	J. Al-Moqyreh	28.8861	35.8778	0	BB
KAMS	Al Khamasin	20.3092	44.5798	75	SP
KBRS	Harrat Khaybar	25.7893	39.2623	78	BB
LBNS	J. Laban	21.0465	39.9013	0	BB
LTHS	Al Lith	20.2750	40.4107	18	BB
MOHS	Muhayl	18.5761	42.0190	52	BB
MYKS	Mirrayikh	21.5545	39.3323	0	SP
MZLS	Mezel	24.0275	45.2071	88	SP
NAJS	Najran	17.5034	44.2847	131	BB
NAMS	Namsa	19.1714	42.2084	252	BB
QURS	Al Hadithat	31.3860	37.3240	49.1	BB
RNYS	Wadi Ranyah	21.4267	42.7662	0	SP
RYDS	Riyadh	24.1900	46.6400	0	BB
TATS	Tathlith	19.5412	43.4775	110	BB
TAYS	Tayyib Ism	28.5511	34.8717	0	BB
TBKS	Tabuk	28.2248	36.5485	82	BB
UMJS	Umm Lajj	25.2340	37.3119	13	SP
WBHS	Wadi-Ibnhashbal	18.6057	42.7144	187	SP
YNBS	Yanbu	24.3397	37.9922	8	BB

These sites are likely affected by nearby cultural noise sources, such as roads and human activities.

Generally, the noise is relatively low between 0.1 and 1 Hz, except for station HASS. Similar results were reported by Mellors (1997). Detection of energy at frequencies around 1 Hz is most important for P-wave arrivals used in the event location. Higher frequency energy is essential for detecting small events at local and regional distance (less than 1,000 km).

Event location analysis

Seismic event location is based on travel times; thus, the accuracy of event location is intimately tied to the accuracy of travel time predictions through seismic velocity models.

Generally, one-dimensional (1D) plane-layered earth models are used in routine event locations, such as the global average model, *iasp91* (Kennett and Engdahl 1991). This model is appropriate for predicting global travel times with a slight bias toward continental (rather than oceanic) observations. However, at local to regional distances (0–1,500 km) travel times are very sensitive to the structure of the crust and uppermost mantle, and accurate prediction of travel times requires regional average or path-specific models. This is demonstrated with observations of two explosions carried out in the Dead Sea in November 1999 (Gitterman and Shapira 2001). These explosions were conducted under tightly controlled conditions so that the location (latitude, longitude, and depth) and origin time are very well known. Table 2 compiles the event information
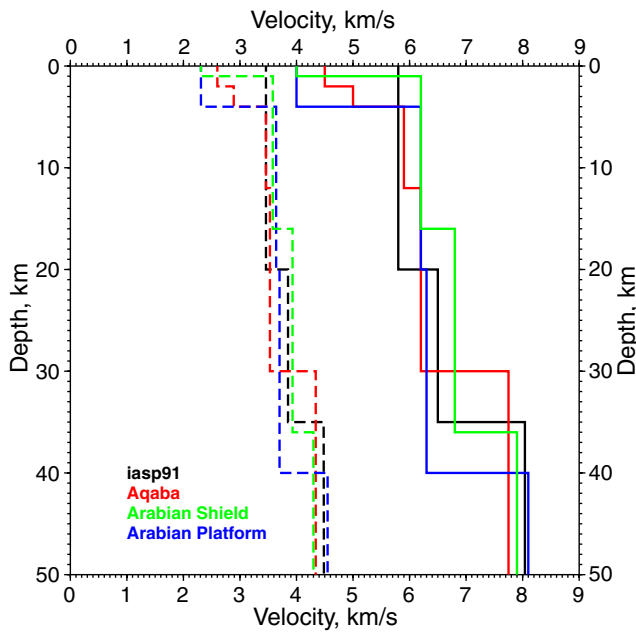
Fig. 3 Seismic P- and S-wave velocity models, *solid* and *dashed*, respectively, for the Arabian Peninsula from various sources described in the text

for these explosions. When arrival times of these events are used to locate these events with the *iasp91* model, the locations are biased by errors in the travel time predictions from the model. Figure 6 shows the locations of the November 10 and 11 Dead Sea explosions, the regional stations that observed the events and the routine locations reported by SANDSN. At the time of these events, the seismic network operated by King Saud University was also operating and observed these events. Note that the SANDSN routine locations of the November 10 and 11 explosions are about 30 and 50 km away from the ground truth locations, respectively. The estimated locations and location errors for these events are compiled in Table 3. Figure 7 shows that vertical component seismograms for the largest (November 11) explosion high-pass filtered at 0.5 Hz. These waveforms show that this event was well observed with high signal-to-noise ratio and very clear arrivals of Pn, Pg, and Sg phases. The crustal S-wave, Sg, is observed on all seismograms, despite the source being an explosion in water. Strong Sg energy may be generated by Rg-to-Sg conversions near the source (Myers et al. 1999). Sn was not clearly observed for these data, including the horizontal components of the KACST network stations. Sn is not expected to propagate efficiently along the paths studied. Previous studies report inefficient Sn propagation in the Dead Sea Rift (Kadinsky-Cade et al. 1981; Rodgers et al. 1997). Inefficient propagation of short-period mantle S-waves probably is due to high attenuation related to low seismic velocities directly below the Moho.

We used these phase travel times (assuming the ground truth location and origin time) to estimate a regional velocity model for the Dead Sea and Gulf of Aqabah region. Data from both shots were included in this analysis. The fact that both explosions have very similar travel times to each station suggests that there are not timing errors at the stations between the two shots. The slopes of the Pg and Sg travel times versus distance should reflect the average P- and S-wave velocities of the crust, while the Pn travel time slope should indicate the average sub-Moho P-wave velocity. However, caution must be exercised because 2D structure along the path could bias the results. In fact, analysis of seismic refraction data sampling the Sinai Peninsula margin of the Gulf of Aqabah indicates that crust thins from about 30 km north of the Gulf to 20 km at the southern-most tip of the Peninsula (Ginzburg et al. 1979). Our goal here is to derive a path-averaged 1D model for the
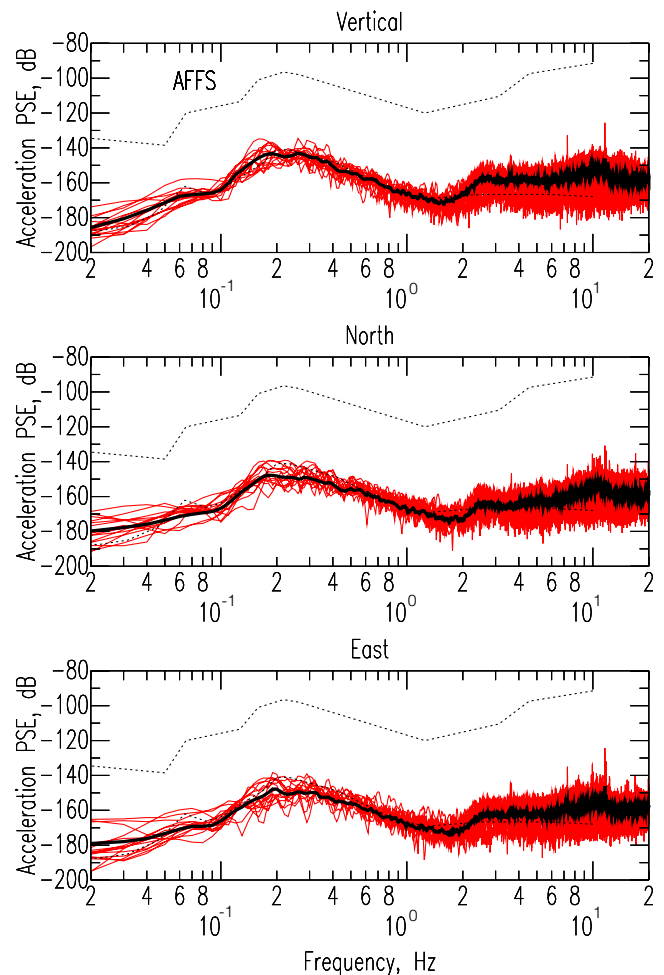

Fig. 4 Noise spectra at station AFFS. Acceleration power spectra (in decibels relative to 1 m2/s4) are shown for the vertical, north and east components. Individual spectra are shown in *red* and the average spectra in *black*. Also shown are the average low and high noise spectra (*dotted line*) of Peterson (1993)
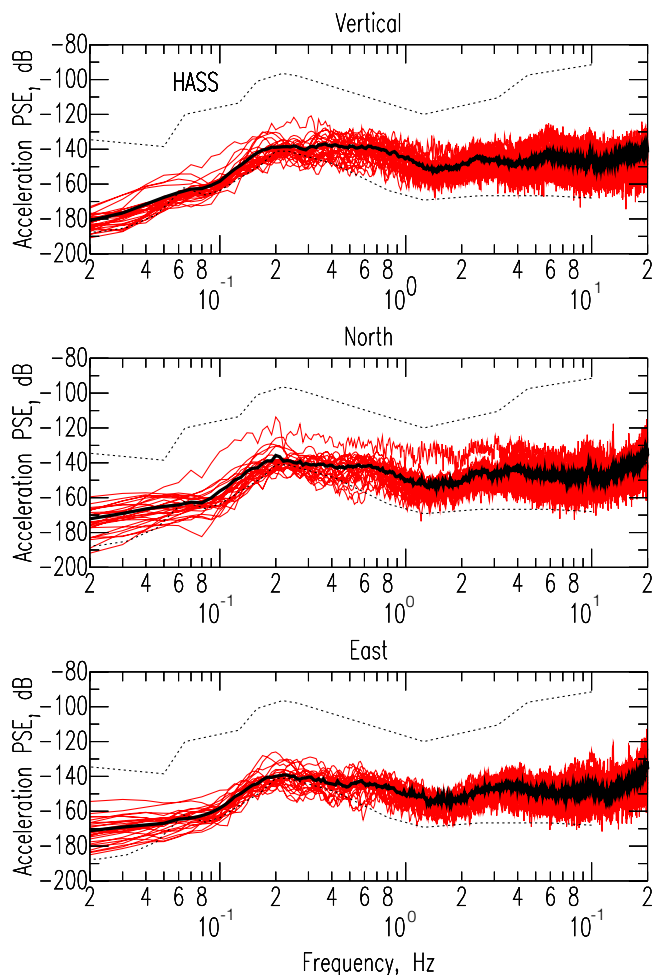
Fig. 5 Noise spectra at station HASS, similar to Fig. 4

paths considered so that future events can be more accurately located.

The slopes of Pg and Sg imply low average crustal velocities (6.28 and 3.43 km/s for P- and S-waves, respectively), consistent with felsic upper crustal compositions of typical continental sections (Christensen and Mooney 1995; Rudnick and Fountain 1995). The average Pn velocity of 7.75 km/s is lower than the global average (8.09 km/s; Christensen and Mooney 1995) but consistent with the seismic refraction study of Ginzburg et al. (1979) and the Pn tomography study of Hearn and Ni (1994). The absence of short-period Sn propagation in the region and low Pn velocities may be consistent with the presence of partial melt in the shallow mantle. The regression fits indicate that the Pn intercept time is quite small (6.03± 1.11 s). This would imply a thin crust (~12 km) and a short Pn–Pg crossover distance (<100 km). However, Pg appears to be the first arrival at station QURS (Fig. 8), implying a thicker crust. A crustal thickness of about 30 km for the Dead Sea region is reported from studies of seismic refraction data (Ginzburg et al. 1979) and teleseismic

receiver functions (Sandvol et al. 1998a, b). The inclusion of data from station QURS may be problematic if the structure to the east of the Dead Sea is dramatically different from that to the south.

Published constraints on crustal structure from previous studies (Rodgers et al. 2003; Al-Damegh et al. 2005; Hansen et al. 2007) report crustal thickness of 25–35 km from receiver function estimates of stations in the region. We were able to model the regional phase travel times with a 30-km-thick crust and relatively low average crustal velocities. Figure 8 shows the fit of the predicted travel times to the observations for the Aqabah model shown in Fig. 3. Also shown are the travel time predictions for the *iasp91* model (Kennett and Engdahl 1991). Note that the travel time differences between the Aqabah and *iasp91* model can be more than a few seconds, and this would result in distance errors of tens of kilometers. We then used the Aqabah model to relocate the events using just the first arriving Pn waves and obtained better locations. Figure 9 shows the improved locations using the Aqabah model, and indeed, the location errors are reduced to 10–20 km. One can expect greater improvement using the later arriving Pg and Sg phases.

To assess bias in the SANDSN event locations for seismogenic regions adjacent to Saudi Arabia, we compared SANDSN locations with well-determined locations based on local, regional, and teleseismic observations. Bondar et al. (2004) demonstrated that the accuracy of event locations can be judged based on the number and azimuthal coverage of observations. Location accuracy is characterized by ground truth or GT level. For example, GT25 events are believed to be located with 25 km of the true location. For this study, we found all events that were determined to be GT25 or better and located by SANDSN. These events are shown in Fig. 10a, where the seismicity clusters into three regions: the Eastern Mediterranean, Zagros, and Gulf of Aden, indicated by the smaller rectangles.
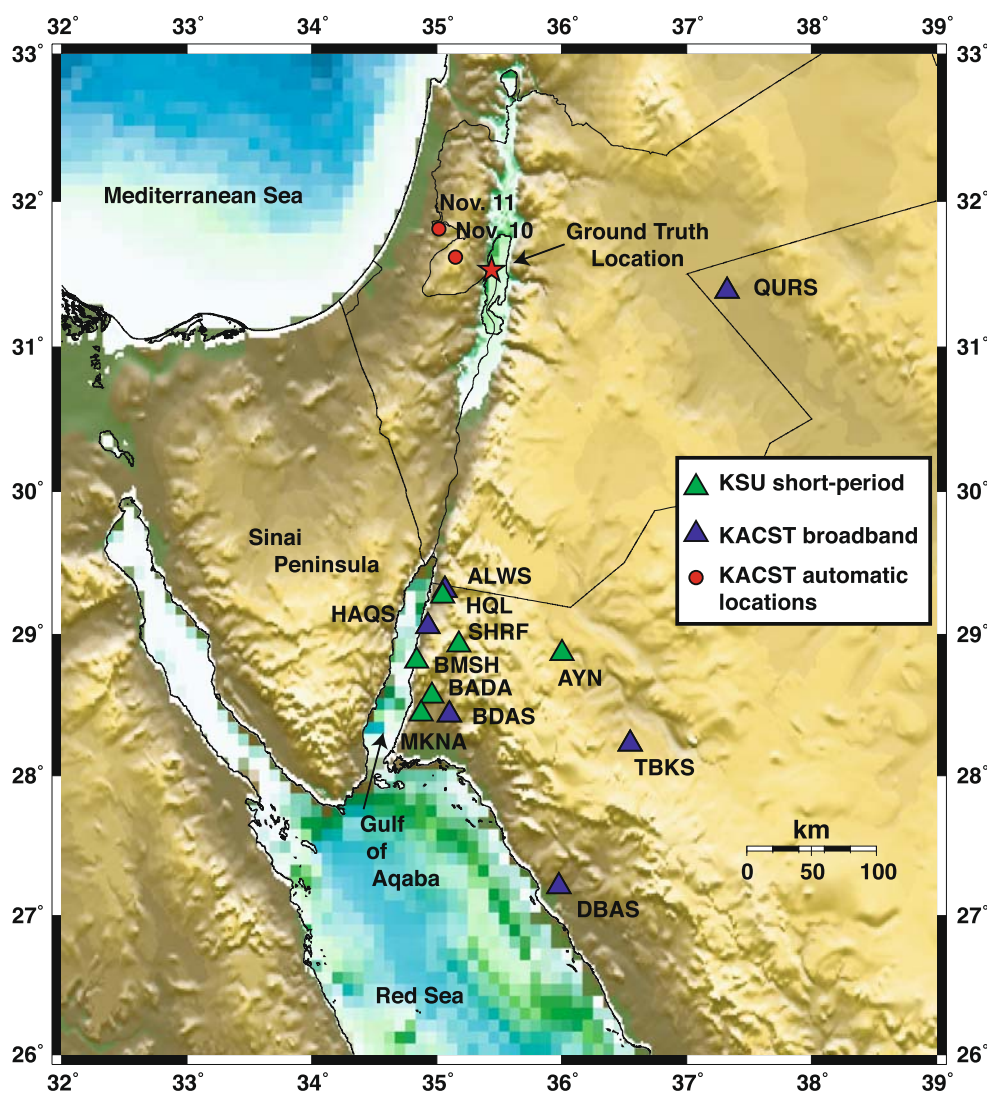
For each cluster of events, we compared the SANDSN and GT locations to investigate possible biases. These comparisons are shown in Fig. 10b–d where we plot the SANDSN location relative to the GT location in polar

Table 2 Ground truth locations from Geophysical Institute of Israel

Latitude	Longitude	Date	Time (GMT)	Yield (kg TNT)
31.5338	35.4400	Nov. 10, 1999	13:59:52.210	2,060
31.5336	35.4413	Nov. 11, 1999	15:00:00.795	5,000

Both shots were detonated in the water at 70–73 m depth.

Fig. 6 Locations of the November 10 and 11 Dead Sea explosions (Gitterman and Shapira 2001) and routine locations using the *iasp91* velocity model. Also shown are the ground truth event locations (*red stars*), estimated event locations (*red circles*), and station locations of the SANDSN (*blue triangles*), and KSU (*green triangles*) networks

coordinates (distance and azimuth). We can see that the SANDSN locations can be off by more than 50 km.

In general, the events are located systematically closer to the SANDSN stations than the GT locations. Events in the Eastern Mediterranean are located to the south, events in the Zagros are located to the southwest, and events in the Gulf of Aden are located to the north. This bias suggests that the true velocity structure is slower than the *iasp91* model. Indeed, our previous work on average velocity models for the Arabian Peninsula determined 1D models for the Arabian Platform and Arabian Peninsula (Rodgers et

al. 1999). These models are plotted along with the *iasp91* model in Fig. 3. These models, including our Aqabah model, show that the crust in the Platform is thicker than for *iasp91* and the mantle in the shield and Gulf of Aqabah regions are much slower than *iasp91*. Improvement in event locations using these models remains for future work.
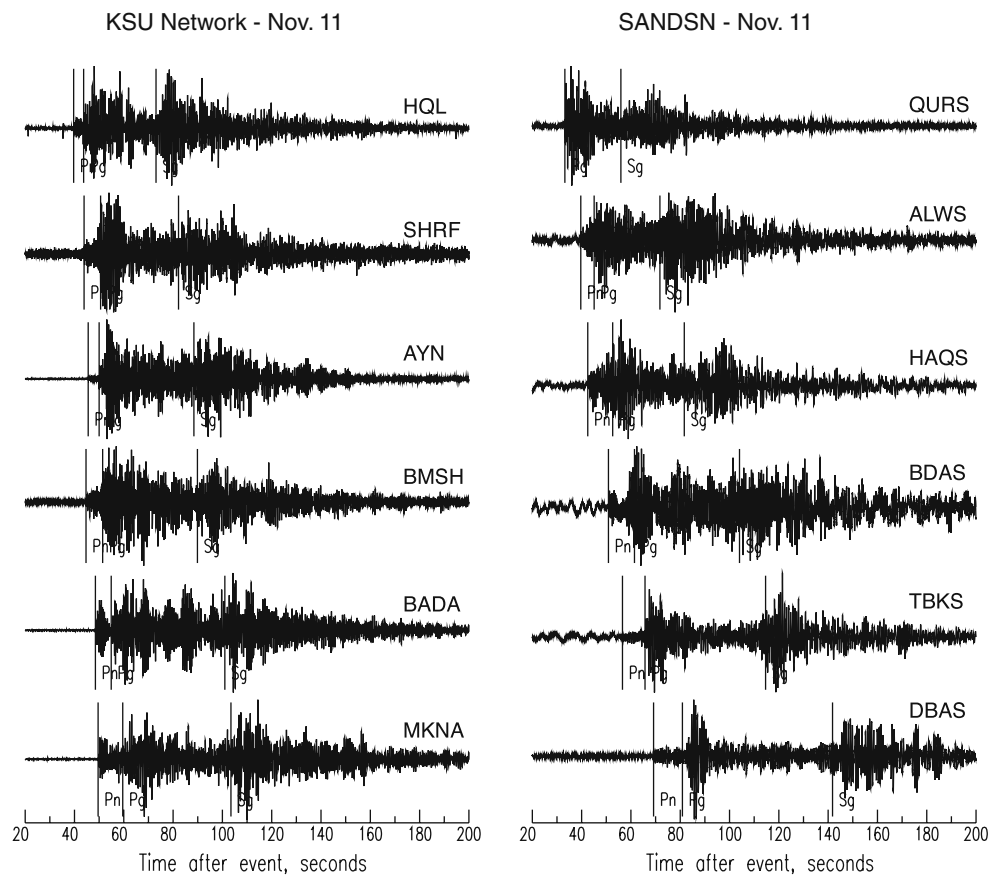
Improved velocity models for the Arabian Peninsula

The sensitivity of travel times to 1D average velocity structure is non-unique. Our initial goal was to find a range of models that fit the data reasonably well and are consistent with what is already known about the region. A grid search (Rodgers et al. 1997, 1999) was used to initially find a range of models that satisfactorily fit the dispersion data. Next, that range of models was explored to fit the three-component broadband (10–100 s) waveforms. The grid search was performed using travel-time data sets: (1) Pn and Pg, and (2) Pn, Pg, and Sg.

Table 3 Automatic locations of Dead Sea shots by Saudi National Seismic Network

Latitude	Longitude	Date	Time (GMT)	Mislocation (km)
31.6214	35.1506	Nov. 10, 1999	13:59:58.807	29.1
31.8143	35.0178	Nov. 11, 1999	14:59:58.572	50.7

Fig. 7 Vertical component seismograms (high-passed filtered at 0.5 Hz) for the largest (November 11, 1999) Dead Sea explosion observed at the KSU and KACST networks. Also shown are analyst picks of the Pn, Pg, and Sg arrivals

Two data sets were considered for two reasons. Firstly, the arrival times of Sg waves were more difficult to pick, and so, it may not be prudent to include them in estimating structure. Secondly, there is a direct solution for the shear-wave velocities, but this required scaling shear velocities to compressional velocities with an assumed Poisson's ratio;
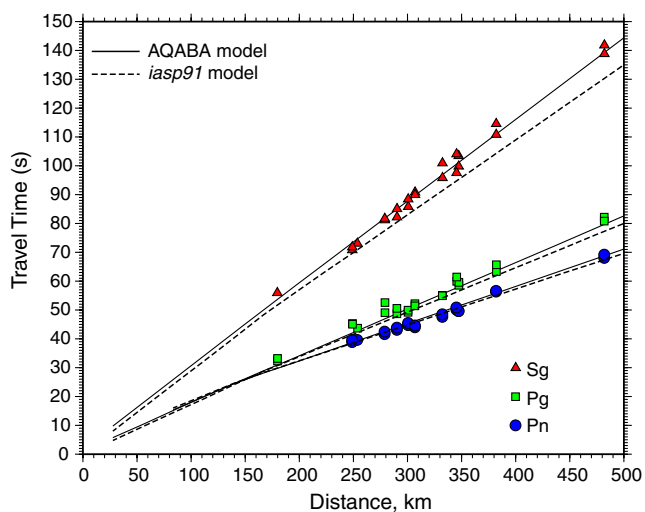

Fig. 8 Observed regional phase travel times for Pn (*blue circles*), Pg (*green squares*), and Sn (*red triangles*) for the two Dead Sea explosions observed at the KACST and KSU networks. Also shown are the travel time predictions of the Aqabah model shown in Fig. 3
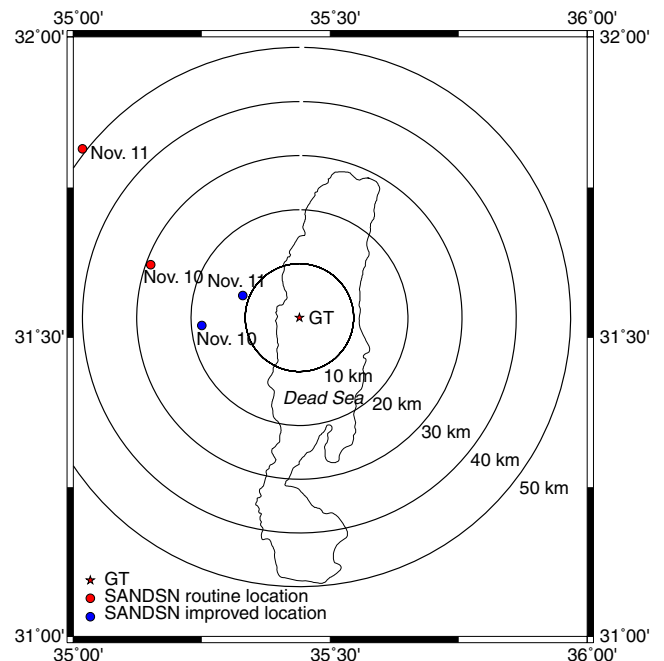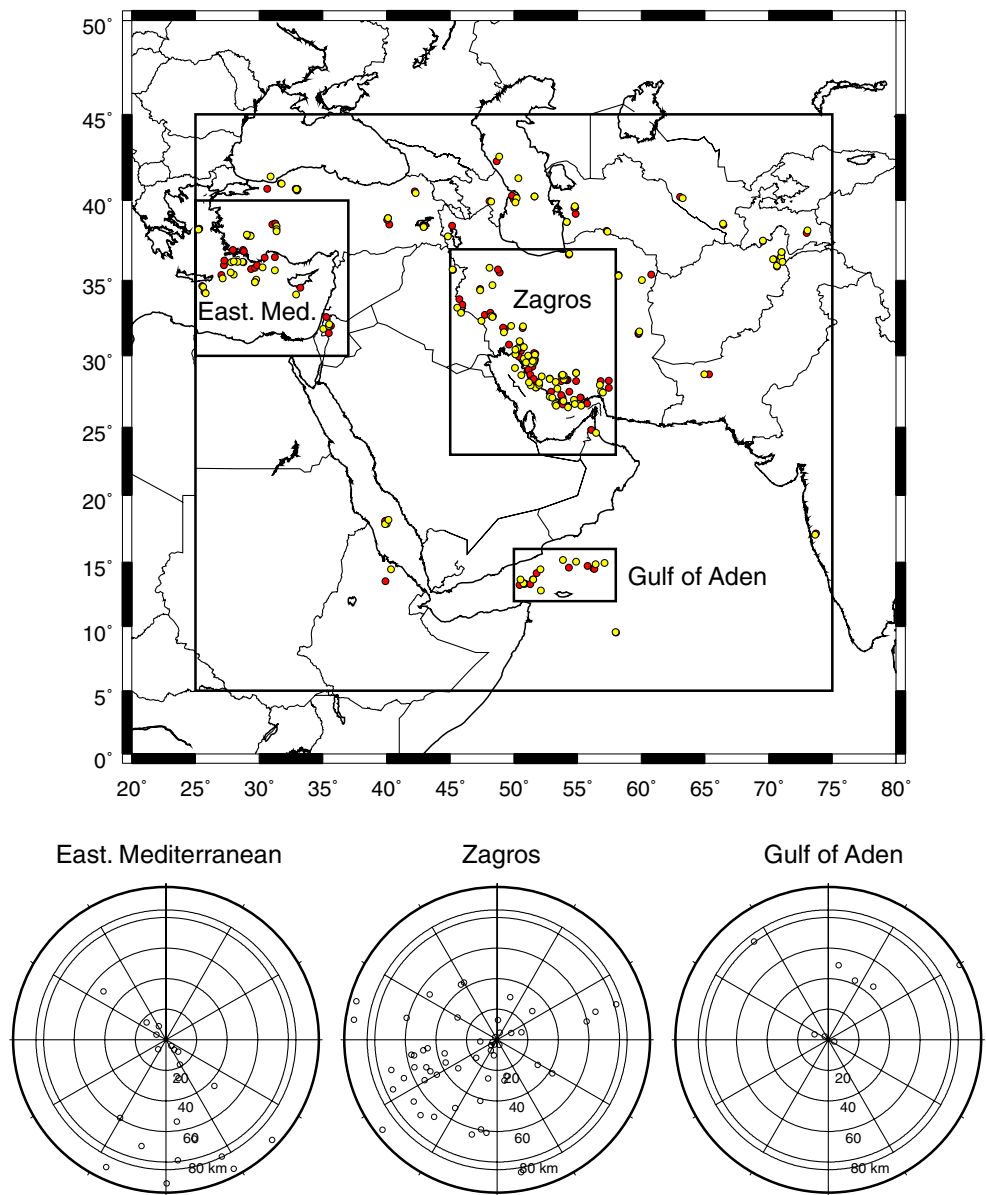

Fig. 9 Ground truth (*red star*) and estimated locations of the two largest Dead Sea explosions, showing both the routine (*red circles*) and improved (*blue circles*) SANDSN locations

Fig. 10 **a** Locations of ground truth (GT, *red*) and SANDSN (*yellow*) events used to evaluate possible location bias. Comparison of SANDSN event locations relative to the GT locations in polar coordinates (distance and azimuth) for three different regions: **b** Eastern Mediterranean; **c** Zagros Mountains and **d** the Gulf of Aden

so, the influence of Sg travel times may bias the model. The optimal model should reduce the scatter in the data (i.e., minimize the root mean square residual, RMS) and result in zero-mean residuals. The models that were chosen resulted in absolute mean residuals of less than 0.5 s and minimum

RMS. The threshold on the absolute mean residual was chosen to be a conservative estimate on the picking error.

From the 800 models considered, the 20 best-fitting models were chosen according to the criteria described above. The crustal thickness was estimated to range between 24 and 30 km. The upper crustal velocities were poorly resolved by both data sets. The velocities of the

Table 4 Velocity model of the Gulf of Aqabah/Dead Sea Region

Depth (km)	Thickness (km)	V_P (km/s)	V_S (km/s)
0	2	4.50	2.60
2	5	5.50	3.18
7	10	6.10	3.52
17	11	6.20	3.60
28	∞	7.80	4.37

V_P and V_S are the P- and S-wave velocities, respectively.

Table 5 Velocity model of the Arabian Shield Region

Depth (km)	Thickness (km)	V_P (km/s)	V_S (km/s)
0	1	4.0	2.31
1	15	6.20	3.58
16	20	6.80	3.93
36	∞	7.90	4.30

Table 6 Velocity model of the Arabian Platform Region

Depth (km)	Thickness(km)	V_P (km/s)	V_S (km/s)
0	4	4.00	2.31
4	16	6.20	3.64
20	20	6.4	3.70
40	∞	8.10	4.55

lower crust are 6.0–6.2 km/s. (Tables 4, 5, and 6). The resulting models revealed significant differences between the lithospheric structure of the three regions.

To check the validity of our model for the Arabian Platform, Rayleigh and Love wave group velocities were measured for a number of regional events in the Zagros Mountains and Turkish–Iranian Plateau. Pathways from these events to the SANDSN stations sample the Arabian Platform. The image shows slower-than-average velocities for the Arabian Platform and Rub' Al-Khali Desert regions, probably due to low-velocity sediment cover. The velocities below the Red Sea are faster-than-average due to the thinner crust. In Saudi Arabia, the 20-s Rayleigh wave group velocities gradually increase from the Eastern Province to the western Hejaz Province and Red Sea. The inclusion of additional surface-wave dispersion data could help resolve the 3D structure in Saudi Arabia.

Ground motion hazards in eastern Saudi Arabia

The most seismically active region near the Kingdom of Saudi Arabia is the Zagros Thrust Belt, where convergence of the Arabian and Eurasian Plates is expressed in frequent earthquakes (Fig. 1). Large (*M*>6.0) events occur on average at least once a year or more frequently in this region; however, these events are 200 km or greater from the Arabian coast. Ground motion hazard for such large distances is unusual. Nonetheless, ground motions caused by distant events in the Zagros have resulted in felt motions in tall buildings in cities along the Arabian coast. An example of this is the November 22, 2005 M 5.7 Qeshm Island. This event caused motions in tall buildings in Dubai, United Arab Emirates, and other cities along the Gulf coast.

Data recorded by the SANDSN allows us to document and understand the nature of these ground motions. Figure 11a shows the location of the Qeshm Island event, focal mechanism, and paths to stations HASS (Al-Hasa, Kingdom of Saudi Arabia) and ZHSF (Iran). The transverse component seismograms from this event recorded at stations HASS and ZHSF, and filtered 0.1–0.3 Hz are shown in Fig. 11b. The paths to these stations should have relatively equal Love-wave radiation due to the paths leaving symmetric sides of the focal mechanism. However, note that the ground motions at HASS are of larger amplitude and longer duration than those at ZHSF. The path to HASS passes through the thick sedimentary cover in the Persian/Arabian Gulf. Similar observations have been seen for other events recorded at HASS. Long-period ground motions are more likely to impact large structures because the resonant period of large structures is longer than small structures.
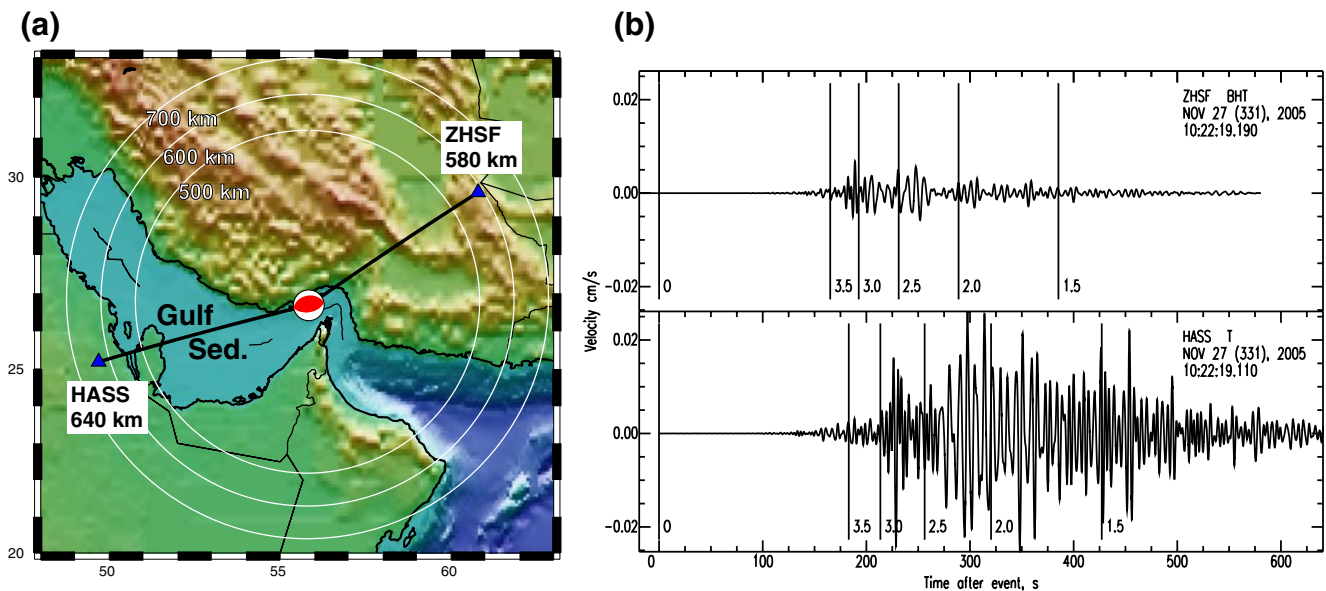

Fig. 11 a Map of the November 27, 2005 Qeshm Island earthquake, focal mechanism and paths to station HASS (Al-Hasa, Eastern Province, Kingdom of Saudi Arabia) and ZHSF (Zahedan, Iran). **b** Transverse component seismograms for the event at ZHSF (*top*) and HASS (*bottom*) filtered 0.1–0.3 Hz

To understand the nature of the long-duration, high-amplitude ground motions, we modeled these seismograms with a 3D model using the spectral element method (SEM) code developed by Komatitsch et al. (2002). We used the 3D model reported by Shapiro and Ritzwoller (2002), which is based on surface wave dispersion and the sedimentary basin thickness reported by Laske and Masters (1997). Figure 12 shows the observed and synthetic seismograms resulting from the SEM calculations for the 3D model and the 1D (or depth-dependent) iasp91 model (Kennett and Engdahl 1991). Note that the 3D model reproduces the character of the observed waveforms with long duration. The 1D model predicts a very simple, short duration surface waveform. This example illustrates that long-duration surface waveforms can be generated from propagation through the thick sedimentary cover in the Gulf.

Conclusions

The SANDSN is an excellent, state-of-the-art seismic network. The sites are quiet, and noise surveys at a few stations indicated that seismic noise levels at SANDSN stations are quite low for frequencies between 0.1 and 1.0 Hz; however, cultural noise appears to affect some stations at frequencies above 1.0 Hz. Broadband waveform data is generally comparable with data from the Global Seismic Network operated by the Incorporated Research Institutions for Seismology.

No Evidence was found of timing problems with the data. The sample rate (currently set at 100 samples/second) can be lowered to 50 samples/second without any loss of information. This would more effectively utilize network communications and computational facilities, and reduce archival storage by a half.

Analysis of broadband seismic waveform from the SANDSN has provided new information for improving seismic hazard assessment in the Arabian Peninsula. The network stations generally have low background noise levels. The development of new velocity models of the crust and upper mantle allow for improved event location, leading to better characterization of seismicity. Preliminary observations of path propagation effects and attenuation indicate that high-frequency ground motions attenuate more rapidly with distance in the Arabian Platform than the Arabian Shield. However, propagation of long-period motions from earthquakes in the Zagros Mountains to the western shore of the Gulf demonstrates high-amplitude and long-duration ground motions. This explains why motions from large and distant events are often felt in tall buildings in the cities along the Gulf coast. The SANDSN provides new and valuable data to investigate seismic hazard in the region. These data will form the basis for much needed future research.

Variability of lithospheric structure was revealed by the requirement for different models for the regions of the northwest of Saudi Arabia (the Gulf of Aqabah and Dead Sea), the Arabian Shield and Platform. Travel-time analysis and surface-wave group velocities confirm the variability in structure and the requirement for path-dependent models.
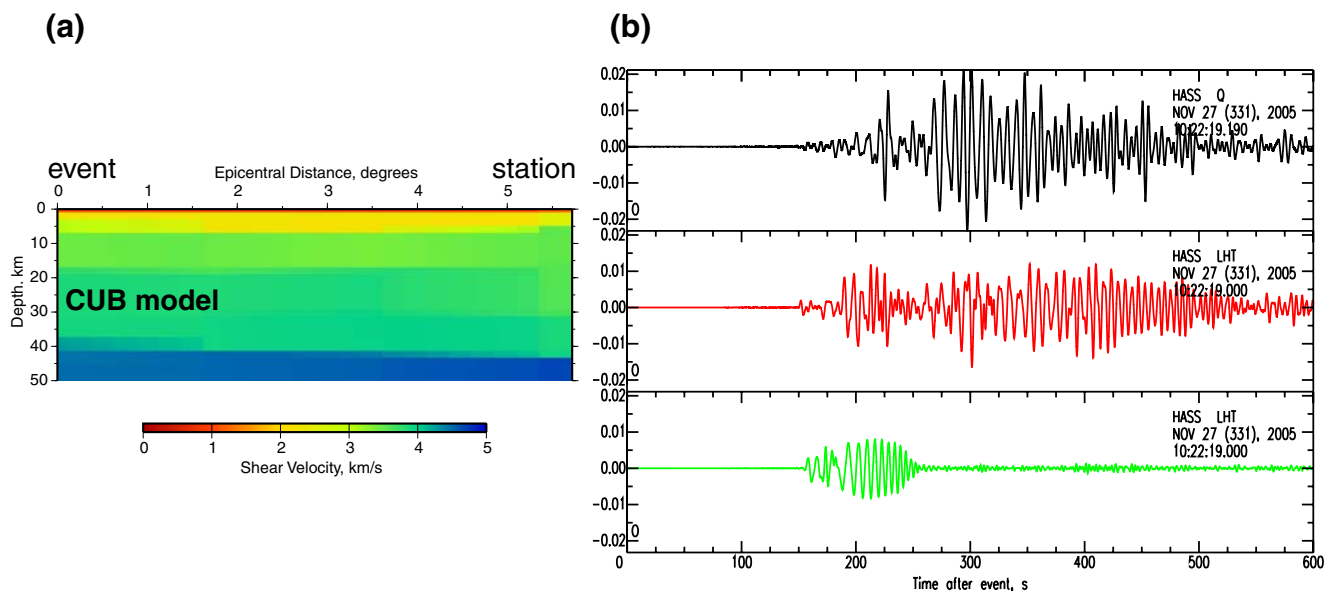

Fig. 12 a Cross-section through the CUB2.0 shear-wave velocity model (Shapiro and Ritzwoller, 2002) along the profile from the Qeshm Island earthquake to station HASS. **b** Transverse component observed (*black*) and synthetic seismograms for the CUB2.0 3D (*red*) and iasp91 1D (*green*) models. Note that the 3D model predicts the amplitude and long duration of the observed response

References

Adams RD, Barazangi M (1984) Seismotectonics and seismology in the Arab region: a brief summary and future plans. Bull Seismol Soc Am 74:1011–1030

Al-Amri AMS (1995) Recent seismic activity in the northern Red Sea. J Geodyn 20:243–253

Al-Amri AM (1998) The crustal structure of the western Arabian Platform from the spectral analysis of long-period P-wave amplitude ratios. Tectonophysics 290:271–283

Al-Amri AM (1999) The crustal and upper-mantle structure of the interior Arabian platform. Geophys J Int 136:421–430

Al-Amri MS, Al-Amri AM (1999) Configuration of the Seismographic networks in Saudi Arabia. Seismol Res Lett 70:322–331

Al-Amri AM, Mellors R, Vernon F (1999) Broadband seismic noise characteristics of the Arabian Shield. Arab J Sci Eng 24(2A):99–113

Al-Damegh K, Sandvol E, Al-Lazki A, Barazangi M (2004) Regional wave propagation (Sn and Lg) and Pn attenuation in the Arabian plate and surrounding regions. Geophys J Int 157:775–795

Al-Damegh K, Sandvol E, Barazangi M (2005) Crustal structure of the Arabian Plate: new constraints from the analysis of teleseismic receiver functions. Earth Planet Sci Lett 231:177–196

Ambraseys NN, Melville CP (1982) A history of Persian earthquakes. Cambridge University Press, London, England, p 219

Ambraseys NN, Melville CP, Adams RD (1994) The seismicity of Egypt, Arabia and the red Sea, a historical review. Cambridge University Press, Cambridge

Badri M (1991) Crustal structure of central Saudi Arabia determined from seismic refraction profiling. Tectonophysics 185:357–374

Benoit M, Nyblade A, VanDecar J, Gurrola H (2003) Upper mantle P wave velocity structure and transition zone thickness beneath the Arabian Shield. Geophys Res Lett 30:1531 doi:10.1029/2002GL016436

Berberian M (1976) Contribution to the seismotectonics of Iran, part II. Geological Survey of Iran, report no. 39, p 516

Bondar I, Myers S, Engdahl ER, Bergman E (2004) Epicenter accuracy based on seismic network criteria. Geophys J Int 156 (3):483–496

Camp VE, Roobol MJ (1992) Upwelling asthenosphere beneath western Arabia and its regional implications. J Geophys Res 97:15255–15271

Christensen N, Mooney W (1995) Seismic velocity structure and composition of the continental crust: a global view. J Geophys Res 100:9761–9788

Cochran JR (1981) Gulf of Aden: Structure and evolution of a young ocean basin and continental margin. J Geophys Res 86:263–287

Debayle E, Leveque J, Cara M (2001) Seismic evidence for a deeply rooted low-velocity anomaly in the upper mantle beneath the northeastern Afro/Arabian continent. Earth Planet Sci Lett 193:423–436

Engdahl ER, Jackson J, Myers S, Bergman E, Priestley K (2006) Relocation and assessment of seismicity in the Iran region. Geophys J Int 167:761–778

Garfunkel Z (1981) Internal structure of the Dead Sea leaky transform (rift) in relation to plate kinematics. Tectonophysics 80:81–108

Gettings M, Blank H, Mooney W, Healey J (1986) Crustal structure of southwestern Saudi Arabia. J Geophys Res 91:6491–6512

Ginzburg A, Makris J, Fuchs K, Prodehl C, Kaminski W, Amitai U (1979) A seismic study of the crust and upper mantle of the Jordan–Dead Sea Rift and their transition toward the Mediterranean Sea. J Geophys Res 84:1569–1582

Girdler RW (1990) The Dead Sea transform fault system. Tectonophysics 180:1–13

Gitterman Y, Shapira A (2001) Dead Sea seismic calibration experiment contributes to CTBT monitoring. Seismol Res Lett 72:159–170

Goldstein P, Dodge D, Firpo M, Miner L (2003) SAC2000: Signal processing and analysis tools for seismologists and engineers. In: Lee WHK, Kanamori H, Jennings PC, Kisslinger C (eds) International handbook of earthquake and engineering seismology. vol. 81B. Academic Press, London, pp 1613–1614

Hansen S, Rodgers A, Schwartz S, Al-Amri A (2007) Imaging ruptured lithosphere beneath the red Sea and Arabian Peninsula. Earth Planet Sci Lett 259:256–265

Hearn T, Ni J (1994) Pn velocities beneath continental collision zones: the Turkish–Iranian Plateau. Geophys J Int 117:273–283

Jackson J, Fitch T (1981) Basement faulting and focal depths of the larger earthquakes in the Zagros mountains (Iran). Geophys J R Astron Soc 64:561–586

Jackson J, McKenzie D (1984) Active tectonics of the Alpine–Himalayan Belt between western Turkey and Pakistan. Geophys J R Astron Soc 77:185–264

Kadinsky-Cade K, Barazangi M, Oliver J, Issacks B (1981) Lateral variations of high-frequency seismic wave propagation at regional distances across the Turkish and Iranian Plateaus. J Geophys Res 86:9377–9396

Kennett B, Engdahl ER (1991) Travel times for global earthquake location and phase identification. Geophys J Int 105:429–465

Klinger Y, Rivera L, Haessler H, Maurin J-C (1999) Active faulting in the Gulf of Aqabah: New knowledge from the MW 7.3 earthquake of 22 November 1995. Bull Seismol Soc Am 89:1025–1036

Komatitsch D, Ritsema J, Tromp J (2002) The spectral-element method, Beowulf computing and global seismology. Science 298:1737–1742

Knopoff L, Fouda A (1975) Upper mantle structure under the Arabian Peninsula. Tectonophysics 26:121–134

Laske G, Masters G (1997) A global digital map of sediment Thickness. EOS Trans AGU 78:F483

Maggi A, Jackson J, Priestley K, Baker C (2000) A re-assessment of focal depth distribution in southern Iran, the Tien Shan and northern India: do earthquakes really occur in the continental mantle? Geophys J Int 43:629–661

Mellors R (1997) Preliminary noise survey and data report of Saudi Arabian data, Lawrence Livermore National Laboratory internal report, UCRL-ID-128949, Office of Scientific and Technical Information, P.O. Box 62, Oak Ridge, TN, 37831, August 2

Mellors R, Vernon F (1999) Analysis of data from the broadband Saudi Arabian deployment, final report to Lawrence Livermore National Laboratory, p 29

Mohsen A, Kind R, Weber M (2006) Thickness of lithosphere at the Dead Sea transform. Geophys J Int 167:845–852

Mokhtar T, Ammon C, Ghalib H, Herrmann R (1997) Lithospheric structure beneath Arabia. EOS 78:F499

Mooney W, Gettings M, Blank H, Healy J (1985) Saudi Arabian seismic refraction profile: a travel time interpretation of crustal and upper mantle structure. Tectonophysics 111:173–246

Myers SC, Walter WR, Mayeda K, Glenn L (1999) Observations in support of Rg scattering as a source of explosion S waves: regional and local recordings of the 1997 Kazakhstan depth of burial experiment. Bull Seismol Soc Am 89:544–549

Nowroozi AA (1972) Focal mechanism of earthquakes in Persia, Turkey, West Pakistan, and Afghanistan, and plate tectonics of the Middle East. Bull Seismol Soc Am 62:823–850

Park Y, Nyblade A, Rodgers A, Al-Amri AM (2007) Upper mantle structure beneath the Arabian Peninsula from regional body-wave tomography: implications for the origin of Cenozoic uplift and volcanism in the Arabian Shield. Geochem Geophys Geosyst 8: Q06021 doi:10.1029/2006GC001566

Peterson J (1993) Observations and modeling of seismic background noise. US Geological Survey Open-File Report 93-322, Albuquerque, New Mexico, p 94

Rodgers A, Ni J, Hearn T (1997) Propagation characteristics of short-period Sn and Lg in the Middle East. Bull Seismol Soc Am 87:396–413

Rodgers A, Walter W, Mellors R, Al-Amri AMS, Zhang YS (1999) Lithospheric structure of the Arabian Shield and Platform from complete regional waveform modeling and surface wave group velocities. Geophys J Int 138:871–878

Rodgers A, Al-Amri A, Ar-Rajehi A, Al-Khalifah T, Al-Amri AM, Al-Haddad M, Al-Arifi N (2001) Analysis of regional travel time data from the November 1999 Dead Sea explosions observed in Saudi Arabia, Lawrence Livermore National Laboratory Informal Document, UCRL-ID-138770

Rodgers A, Harris D, Ruppert S, Lewis JP, O'Boyle J, Pasyanos M, Fandi Abdallah AQ, Al-Yazjeen T, Al-Gazo A (2003) A broadband seismic deployment in Jordan. Seism Res Lett 74:374–381

Rudnick R, Fountain D (1995) Nature and composition of the continental crust: a lower crustal perspective. Rev Geophys 33:267–309

Sandvol E, Seber D, Barazangi M, Vernon F, Mellors R, Al-Amri A (1998a) Lithospheric seismic velocity discontinuities beneath the Arabian Shield. Geophys Res Lett 25:2873–2876

Sandvol E, Seber D, Calvert A, Barazangi M (1998b) Grid search modeling of receiver functions: implications for crustal structure in the Middle East and North Africa. J Geophys Res 103:26899–26917

Seber D, Mitchell B (1992) Attenuation of surface waves across the Arabian Peninsula. Tectonophysics 204:137–150

Seber D, Vallve M, Sandvol E, Steer D, Barazangi M (1997) Middle East tectonics: applications of geographical information systems (GIS). GSA Today February:1–5

Shapiro NM, Ritzwoller MH (2002) Monte-Carlo inversion for a global shear velocity model of the crust and upper mantle. Geophys J Int 151:88–105

Stocklin J (1968) Structural history and tectonics of Iran: a review. Bull Am Assoc Petrol Geol 52:1229–1258

Stoeser D, Camp V (1985) Pan-African microplate accretion of the Arabian shield. Geol Soc Am Bull 96:817–826

Sweeney J (1996) Accuracy of teleseismic event locations in the Middle East and North Africa, Lawrence Livermore National Laboratory, Technical Report, UCRL-ID-125868, Livermore, CA, USA

Tiberi C, Leroy S, D'Acremont E, Bellahsen N, Ebinger C, Al-Lazki A, Pointu A (2007) Crustal geometry of the northeastern Gulf of Aden passive margin: localization of the deformation inferred from receiver function analysis. Geophys J Int 168:1247–1260

Tkalčič H, Pasyanos M, Rodgers A, Gok R, Al-Amri A (2006) A multi-step approach for joint modeling of surface wave dispersion and teleseismic receiver functions: implications for lithospheric structure of the Arabian Peninsula. J Geophys Res 111: B113111 doi:10.1029/2005JB004130

Vernon F, Berger J (1998) Broadband seismic characterization of the Arabian Shield, Final Scientific Technical Report, Department of Energy Contract No. F 19628-95-K-0015, p 36